A study of electroweak vacuum metastability with a singlet scalar dark matter

Najimuddin Khan[†1] and **Subhendu Rakshit**[†2]

[†]*Discipline of Physics, Indian Institute of Technology Indore, IET-DAVV Campus, Indore 452017, India*

Abstract

We study several aspects of electroweak vacuum metastability when an extra gauge singlet scalar, a viable candidate for a dark matter particle, is added to the standard model of particle physics, which is assumed to be valid up to the Planck scale. Phase diagrams are drawn for different parameter spaces, and based on that, we graphically demonstrate how the confidence level, at which stability of electroweak vacuum is excluded, depends on such new physics parameters.

arXiv:1407.6015v2 [hep-ph] 6 Nov 2014

[1]phd11125102@iiti.ac.in
[2]rakshit@iiti.ac.in

1 Introduction

The recent discovery of the Higgs boson at 125.66 ± 0.3 GeV [1–3] completes search for the particle content of the standard model (SM), confirming Higgs mechanism to be responsible for electroweak symmetry breaking. It brings forward the issue of naturalness, indicating the presence of new physics at the $\sim$ TeV scale.

LHC, with $20\,\text{fb}^{-1}$ data in its $\sqrt{s} = 8$ TeV run, is yet to find any such hint of new physics. Hence, it looks like infrared naturalness [4] is not the right guiding principle for hunting physics beyond SM, and, new ideas are required to understand hierarchy problem. It is possible that SM is not an effective theory but a fundamental theory of Nature, valid up to the Planck scale ($M_{\rm Pl}$), where quantum gravity effects kick off.

In such a scenario, Higgs boson mass $M_H \sim 126$ GeV is consistent with $\lambda(M_{\rm Pl}) \sim 0$, *i.e.,* with vanishing self-coupling of Higgs boson at $M_{\rm Pl}$. In addition, as the beta function

$$\beta_{M_H^2} = \frac{d\, M_H^2(\mu)}{d\, \ln \mu}$$

is proportional to M_H^2, the smallness of the Higgs mass would be ensured if $M_H(M_{\rm Pl}) \sim 0$ [4, 5]. All these indicate a vanishing Higgs potential near $M_{\rm Pl}$, which perhaps is ensured by Planck scale physics. The exact mechanism for this is unknown, as we do not expect to understand the dynamics at this regime in the context of a conventional perturbative quantum field theory. So in the quantum corrections to the Higgs mass, putting the cut-off scale $\Lambda \to M_{\rm Pl}$ does not make any sense. If $M_{\rm Pl}$ does not get introduced in the theory as a physical scale [5], there is no hierarchy problem to start with. So, smallness of Higgs mass may rather be ensured by ultraviolet naturalness [4] than the usual infrared naturalness: The quadratic divergences might be spurious [5, 6], as we are looking from the electroweak scale than the Planck scale which possibly hold the key of ensuring naturalness.

For Higgs field values much greater than the electroweak (EW) vacuum, the Higgs effective potential [7, 8] turns down due to large contributions from top quark loops. As a result, there might exist a second minimum of the potential around $M_{\rm Pl}$. If this minimum is significantly deeper than the EW minimum, the vacuum transition probability can be sizable, threatening the fate of this Universe. Given the present uncertainties of SM parameters, the EW vacuum is metastable at 99.3% CL [9].

Stability of the potential is ensured if the two vacua are at the same level, namely

$$V(\phi_{\rm EW}) = V(\phi_{\rm new}) \quad \text{and} \quad V'(\phi_{\rm EW}) = V'(\phi_{\rm new}) = 0\,,$$

where, $\phi_{\rm EW}$ and $\phi_{\rm new}$ correspond respectively to the EW vacuum and the new vacuum at a very large value of the field. Neglecting quantum corrections of $\mathcal{O}(\alpha)$, this corresponds to the conditions [10]

$$\lambda(\Lambda_0) = \beta_\lambda(\Lambda_0) = 0\,, \qquad \beta_\lambda(\mu) = \frac{d\,\lambda(\mu)}{d\, \ln \mu}\,, \tag{1}$$

where Λ_0 is some energy scale in between the EW scale and $M_{\rm Pl}$, at which the instability starts setting in.

Recent cosmological and astrophysical evidences suggest presence of cold dark matter (DM), which cannot be explained in the scenario described above. A simple choice is to add a gauge singlet real scalar S to the SM [11]. An additional $\mathbb{Z}_2$ symmetry ensures the stability of S. The scalar modifies the Higgs effective potential, and can ensure vacuum stability up to $M_{\rm Pl}$.

Such extensions of SM have been discussed in the literature in the context of vacuum stability. In a model SM+S, where SM is extended by a scalar DM, whether the boundary conditions $\lambda = 0$, $\beta_\lambda = 0$ and the Veltman condition are satisfied at $M_{\rm Pl}$ is discussed in ref. [12] (see also refs. [13–15]). It is shown that the correct DM relic density is obtained if DM mass lies in the range 300 GeV $\lesssim M_S \lesssim$ 1 TeV. Introduction of a scalar relaxes [16] Higgs mass bounds stemming from vacuum stability considerations and perturbativity. Such constraints were also considered in SM+S model, in the context of inflation, where either Higgs [17] or the scalar S [18] acts as an inflaton. Model dependence of Higgs mass bounds were discussed in ref. [19] using a two-loop analysis for models with additional spin 0 and 1/2 electroweak singlet, doublet and triplets. Vacuum stability in a scalar extended SM has been explored in refs. [20, 21] where the scalar is allowed to mix with the Higgs. In a more elaborate model consisting of a complex scalar and two fermions, where one of the fermions serve as a DM particle, issues pertaining to vacuum stability have been discussed in ref. [22]. Vacuum metastability constraints in the context of seesaw models have been discussed in refs. [14, 23]. Planck scale dynamics is expected to affect stability of EW vacuum. This has been demonstrated in refs. [24–27] incorporating higher dimensional operators suppressed by $M_{\rm Pl}$ in the Higgs potential. Similar study in scalar DM model was performed in ref. [28].

While the existing literature mainly concentrates on constraints ensuing from the stability of the Higgs effective potential, the possibility that the EW vacuum remains in the metastable state even after adding the scalar has not been discussed in depth. Although, in the context of SM, detailed studies of metastability exist in the literature [9, 10, 29, 30]. Along the same line, in this paper, we extend studies of the metastable vacuum in the SM+S model. In particular, we provide quantitative measures of metastability in terms of tunneling probability and confidence level plots.

The paper is organised as follows. In Section 2 we deal with theoretical aspects of SM+S model with a discussion on RGE running of various couplings and the Higgs effective potential. Tunneling probability of EW vacuum is discussed in Section 3, followed by presentation of phase diagrams in different parameter spaces in Section 4. Finally we conclude in Section 5.

2 Effective potential and RGE running

An extra real scalar singlet field S, odd under $\mathbb{Z}_2$ symmetry, is added to the SM, providing a suitable candidate for dark matter. The corresponding Lagrangian density is given by,

$$\mathcal{L}_S = \frac{1}{2}(\partial_\mu S)(\partial^\mu S) - V_0^S \tag{2}$$

with,

$$V_0^S = \frac{1}{2}\overline{m}_S^2 S^2 + \frac{\kappa}{2}|\Phi|^2 S^2 + \frac{\lambda_S}{4!}S^4\,,$$

where,

$$\Phi = \begin{pmatrix} G^+ \\ (\phi + v + iG^0)/\sqrt{2} \end{pmatrix}.$$

After spontaneous EW symmetry breaking, DM mass M_S is expressed as $M_S^2 = \overline{m}_S^2 + \kappa v^2/2$.

SM tree level Higgs potential

$$V_0^{\rm SM}(\phi) = -\frac{1}{2}m^2\phi^2 + \frac{1}{4}\lambda\phi^4 \tag{3}$$

is augmented by the SM+S one-loop Higgs potential in Landau gauge using $\overline{\rm MS}$ scheme, which is written as

$$V_1^{{\rm SM}+S}(\phi) = V_1^{\rm SM}(\phi) + V_1^S(\phi) \tag{4}$$

with [18, 31],

$$\begin{aligned} V_1^{\rm SM}(\phi) &= \sum_{i=1}^{5} \frac{n_i}{64\pi^2} M_i^4(\phi)\left[\ln\frac{M_i^2(\phi)}{\mu^2(t)} - c_i\right] \\ V_1^S(\phi) &= \frac{1}{64\pi^2} M_S^4(\phi)\left[\ln\left(\frac{M_S^2(\phi)}{\mu^2(t)}\right) - \frac{3}{2}\right] \end{aligned}$$

where n_i is the number of degrees of freedom. For scalars and gauge bosons, n_i comes with a positive sign, whereas for fermions it is associated with a negative sign. Here $c_{H,G,f} = 3/2$, $c_{W,Z} = 5/6$ and $\mu(t) = M_Z \exp(t)$. $M_i(\phi)$ and $M_S(\phi)$ are given by

$$M_i^2(\phi) = \kappa_i(t)\phi^2(t) - \kappa_i'(t) \qquad \text{and} \qquad M_S^2(\phi) = \overline{m}_S^2(t) + \kappa(t)\phi^2(t)/2\,.$$

n_i, κ_i and κ_i' can be found in eqn. (4) in ref. [32] (see also refs. [33–36]). In this paper, in the Higgs effective potential, SM contributions are taken at two-loop level [9, 29, 37, 38], whereas the scalar contributions are considered at one-loop only.

For $\phi \gg v$, the effective potential can be approximated as

$$V_{\rm eff}^{{\rm SM}+S}(\phi) \simeq \lambda_{\rm eff}(\phi)\frac{\phi^4}{4}\,, \tag{5}$$

with

$$\lambda_{\rm eff}(\phi) = \lambda_{\rm eff}^{\rm SM}(\phi) + \lambda_{\rm eff}^{S}(\phi)\,,$$

where [9, 31],

$$\begin{aligned}
\lambda_{\rm eff}^{\rm SM}(\phi) &= e^{4\Gamma(\phi)}\left[\lambda(\mu=\phi) + \lambda_{\rm eff}^{(1)}(\mu=\phi) + \lambda_{\rm eff}^{(2)}(\mu=\phi)\right] \\
\lambda_{\rm eff}^{S}(\phi) &= e^{4\Gamma(\phi)}\left[\frac{\kappa^2}{64\pi^2}\left(\ln\left(\frac{\kappa}{2}\right) - \frac{3}{2}\right)\right]\,.
\end{aligned}$$

Here

$$\Gamma(\phi) = \int_{M_t}^{\phi} \gamma(\mu)\, d\, \ln\mu\,.$$

Anomalous dimension $\gamma(\mu)$ of the Higgs field takes care of its wave function renormalisation. As quartic scalar interactions do not contribute to wave function renormalisation at one-loop level, S does not alter $\gamma(\mu)$ of SM and anomalous dimension of S is zero [16]. The expressions for the one- and two-loop quantum corrections $\lambda_{\rm eff}^{(1,2)}$ in SM can be found in ref. [9]. All running coupling constants are evaluated at $\mu = \phi$.

For RGE running, we use three-loop SM beta functions [9, 39–43] for g_1, g_2, g_3, y_t and λ. For $\mu \geq M_S$, β_λ receives a correction [12] $\kappa^2/2$ at one-loop due to S. The beta functions for the new physics parameters κ and λ_S are given by [12, 17, 44]

$$\beta_\kappa = \begin{cases} 0 & \text{for } \mu < M_S \\ \kappa\left[4\kappa + 12\lambda + 6y^2 - \frac{3}{2}(g'^2 + 3g^2) + \lambda_S\right] & \text{for } \mu \geq M_S \end{cases}\,, \tag{6}$$

$$\beta_{\lambda_S} = \begin{cases} 0 & \text{for } \mu < M_S \\ 3\lambda_S^2 + 12\kappa^2 & \text{for } \mu \geq M_S \end{cases}\,. \tag{7}$$

$\overline{m}_S$ also evolves with energy. But as the beta functions of other parameters do not involve $\overline{m}_S$, we do not consider its beta function in this discussion. Here, new physics effects are included in the RGEs at one-loop only.

2.1 RGE running from $\mu = M_t$ to $M_{\rm Pl}$

We evaluate the coupling constants at the highest mass scale of the SM namely the top quark mass M_t and then run them according to the RGEs up to the Planck scale. To know their values at M_t, one needs to take into account various threshold corrections up to M_t [45–47]. All coupling constants are expressed in terms of pole masses [10]. To calculate $g_1(M_t)$ and $g_2(M_t)$, one-loop RGEs are enough. For $g_3(M_t)$, we first use three-loop RGE running of α_s with five flavours excluding the top quark, and, then the effect of top is included using prescriptions of an effective field theory. The leading term in four-loop RGE for α_S is also taken into account. Amongst all Yukawa couplings, the running of y_t is the most significant. $\overline{\rm MS}$ y_t is related to the

top pole mass M_t by the matching condition $y_t(M_t) = \frac{\sqrt{2}M_t}{v}(1 + \delta_t(M_t))$. In $\delta_t(M_t)$, we take into account three-loop QCD, one-loop electroweak, and two-loop $\mathcal{O}(\alpha\alpha_S)$ corrections. Similarly, the relation between $\overline{\rm MS}$ λ and Higgs pole mass M_H is given by $\lambda(M_t) = \frac{M_H^2}{2v^2}(1 + \delta_H(M_t))$. In $\delta_H(M_t)$, we consider one-loop electroweak, two-loop $\mathcal{O}(\alpha\alpha_S)$, two-loop $\mathcal{O}(y_t^4 g_3^2)$ and two-loop $\mathcal{O}(y_t^6)$ corrections. The loop effects considered in these matching conditions are comparable to refs. [10, 29]. After knowing the values of various coupling constants at M_t, we use full three-loop SM RGEs and one-loop RGEs for the scalar S to run them up to $M_{\rm Pl}$.

Using these matching conditions, in Table 1 we find different coupling constants at $M_t = 173.1$ GeV and at $M_{\rm Pl}$ with $M_H = 125.66$ GeV and $\alpha_s(M_Z) = 0.1184$. As we are considering running all the way up to the Planck scale, the values at very high energies are extremely sensitive to the initial values at M_t. Hence, significant places of decimals are provided to enable the reader to reproduce the running.

μ (GeV)	g_1	g_2	g_3	y_t	λ
M_t	0.358725	0.648184	1.16449	0.935644	0.126971
$M_{\rm Pl}$	0.476006	0.506548	0.488986	0.384124	−0.0123196

Table 1: *Values of all* SM *coupling constants at* M_t *and* $M_{\rm Pl}$ *for* $M_t = 173.1$ *GeV,* $M_H = 125.66$ *GeV and* $\alpha_S(M_Z) = 0.1184$.

For SM+S, the running depends on the extra parameters M_S, $\kappa(M_Z)$ and $\lambda_S(M_Z)$. Assuming the values of SM parameters at M_t as given in Table 1, we present values of all parameters at $M_{\rm Pl}$ in SM+S model in Table 2, for two different sets of M_S, $\kappa(M_Z)$ and $\lambda_S(M_Z)$. The first set stands for our benchmark point, as described later. For this choice, $\lambda(M_{\rm Pl})$ is negative. The second set is chosen such that $\lambda(M_{\rm Pl}) = 0$. Note that as we do not consider running of new physics parameters till M_S, in our case it is all the same to specify these parameters either at M_Z or at M_t.

M_S	$\kappa(M_Z)$	$\lambda_S(M_Z)$	g_1	g_2	g_3	y_t	λ	κ	λ_S
620	0.185	1	0.478	0.506	0.487	0.382	−0.0029	0.424	4.66
795	0.239	0.389	0.478	0.506	0.487	0.382	0	0.412	1

Table 2: *Values of all* SM+S *coupling constants at* $M_{\rm Pl} = 1.2 \times 10^{19}$ *GeV with* $M_t = 173.1$ *GeV,* $M_H = 125.66$ *GeV and* $\alpha_S(M_Z) = 0.1184$.

In the SM, the gauge couplings g_1, g_2, g_3, top Yukawa coupling y_t do not vanish at $M_{\rm Pl}$. The same is true in SM+S model [15], since running of these couplings are hardly affected by S, as displayed in Fig. 1. Higgs portal coupling κ and scalar self-quartic coupling λ_S increase with energy. The rise of λ_S is so rapid that it may

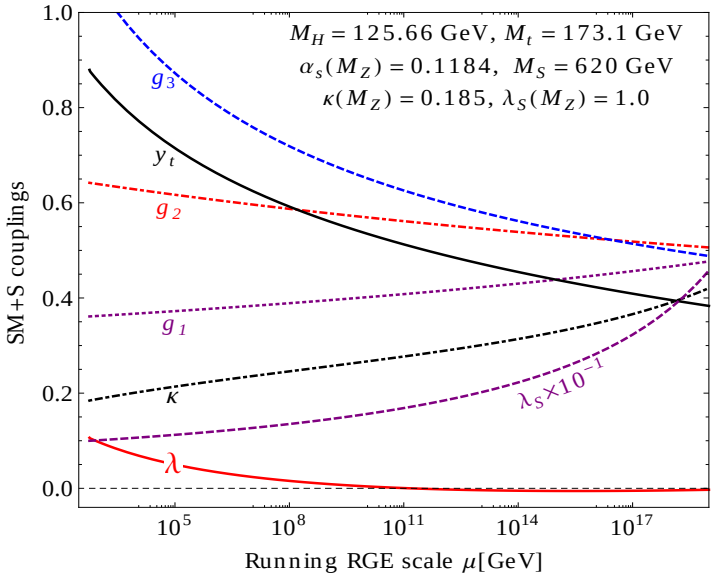

Figure 1: SM+S *RG evolution of the gauge couplings* g_1, g_2, g_3*, top Yukawa coupling* y_t*, Higgs self-quartic coupling* λ*, Higgs portal coupling* κ *and scalar self-quartic coupling* λ_S *in* $\overline{\text{MS}}$ *scheme.*

render the theory nonperturbative at higher energies. For example, if $\lambda_S(M_Z) > 1.3$, λ_S becomes nonperturbative before $M_{\rm Pl}$. Higgs self-quartic coupling λ also gets affected by inclusion of S. But the change is not visible in Fig. 1.

As the issue of stability hinges on the value of λ at higher energies, we focus on the running of λ both in SM and SM+S models in Fig. 2. In SM, λ becomes vanishingly small and negative at energies before $M_{\rm Pl}$, signifying the possible presence of new physics. λ crosses zero at a scale Λ_I, where the instability starts setting in. Considering central values for M_t, M_H and $\alpha_S(M_Z)$, $\Lambda_I \sim 1.9 \times 10^{10}$ GeV in the SM. We display the same curve for SM+S in Fig. 2(b), for a *benchmark point* $M_S = 620$ GeV, $\kappa(M_Z) = 0.185$ and $\lambda_S(M_Z) = 1$. We observe that the behaviour of λ running might change significantly, modifying Λ_I to 1.68×10^{11} GeV. It has the potential to push out the EW vacuum from metastability to a stable vacuum. The benchmark point is chosen keeping in mind that the new physics effects are clearly visible, yet the vacuum is still in metastable state. This point also satisfies the Planck and WMAP imposed DM relic density constraint $\Omega_{\rm DM}h^2 = 0.1198 \pm 0.0026$ [48]. We use `FeynRules` [49] along with `micrOMEGAs` [50,51] to compute relic density of scalar DM in SM+S model.

As defined in eqn. (5), $\lambda_{\rm eff}$ differs from λ as it takes care of loop corrections. In the SM, in ref. [29] it was shown that the difference $\lambda_{\rm eff} - \lambda$ is always positive and negligible near $M_{\rm Pl}$. We see in Fig. 3(a) that SM+S exhibit similar features. However, the instability scale Λ_I changes significantly if we choose to work with $\lambda_{\rm eff}$

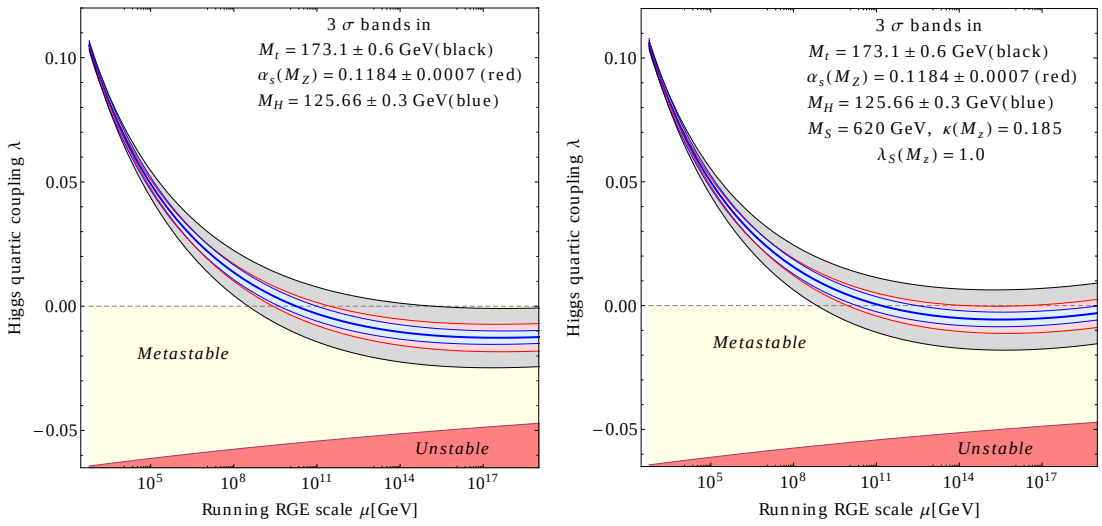
3 σ bands in
$M_t = 173.1 \pm 0.6$ GeV(black)
$\alpha_s(M_Z) = 0.1184 \pm 0.0007$ (red)
$M_H = 125.66 \pm 0.3$ GeV(blue)
Higgs quartic coupling λ
Metastable
Unstable
Running RGE scale μ[GeV]
3 σ bands in
$M_t = 173.1 \pm 0.6$ GeV(black)
$\alpha_s(M_Z) = 0.1184 \pm 0.0007$ (red)
$M_H = 125.66 \pm 0.3$ GeV(blue)
$M_S = 620$ GeV, $\kappa(M_z) = 0.185$
$\lambda_S(M_z) = 1.0$
Higgs quartic coupling λ
Metastable
Unstable
Running RGE scale μ[GeV]

(a) (b)

Figure 2: (**a**) *RG evolution of* λ *in the* SM. (**b**) *RG evolution of* λ *in the* SM+S *for our benchmark point. In both panes* 3σ *bands for* M_t, M_H *and* $\alpha_s(M_Z)$ *are displayed.*

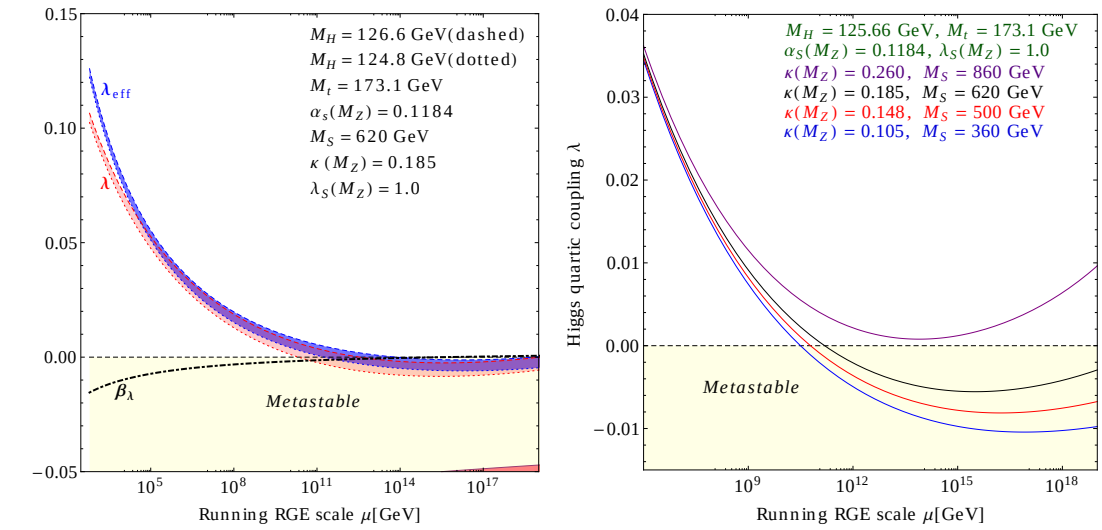
$M_H = 126.6$ GeV(dashed)
$M_H = 124.8$ GeV(dotted)
$M_t = 173.1$ GeV
$\alpha_s(M_Z) = 0.1184$
$M_S = 620$ GeV
$\kappa(M_Z) = 0.185$
$\lambda_S(M_Z) = 1.0$
$\lambda_{\rm eff}$
λ
β_λ
Metastable
Running RGE scale μ[GeV]
$M_H = 125.66$ GeV, $M_t = 173.1$ GeV
$\alpha_S(M_Z) = 0.1184$, $\lambda_S(M_Z) = 1.0$
$\kappa(M_Z) = 0.260$, $M_S = 860$ GeV
$\kappa(M_Z) = 0.185$, $M_S = 620$ GeV
$\kappa(M_Z) = 0.148$, $M_S = 500$ GeV
$\kappa(M_Z) = 0.105$, $M_S = 360$ GeV
Higgs quartic coupling λ
Metastable
Running RGE scale μ[GeV]

(a) (b)

Figure 3: (**a**) *RG evolution of* λ *(red band),* $\lambda_{\rm eff}$ *(blue band) and* β_λ *(dot-dashed black) in* SM+S *for our benchmark point.* (**b**) *Evolution of* λ *for different* $\kappa(M_Z)$*. Each* $\kappa(M_Z)$ *corresponds to a specific* M_S *to satisfy DM relic density* $\Omega_{\rm DM}h^2 \approx 0.1198$*.*

instead of λ: In SM, the instability scale changes to 1.25×10^{11} GeV and in SM+S, it becomes 1.7×10^{12} GeV. We also plot β_λ to show that at high energies, λ, $\lambda_{\rm eff}$ and β_λ all seem to vanish.

In Fig. 3(b) we display RGE running of λ for various new physics parameters to explicitly demonstrate that as $\kappa(M_Z)$ increases, for a given energy, λ assumes a higher value [13, 14]. Finally, for some parameter space, λ never turns negative, implying stability of the EW vacuum. It happens due to the $\kappa^2/2$ term in β_λ. Due to this positive contribution, the presence of the scalar never drives EW vacuum towards instability. Next, we will calculate the tunneling probability to demonstrate stability issues with EW vacuum.

3 Tunneling probability

The present data on M_H and M_t indicate that the Universe might be residing in a false vacuum, waiting for a quantum tunneling to a true vacuum lying close to the Planck scale.

The vacuum decay probability of EW vacuum at the present epoch is given by [9, 52, 53]

$$\mathcal{P}_0 = 0.15 \frac{\Lambda_B^4}{H_0^4} e^{-S(\Lambda_B)} \tag{8}$$

where,

$$S(\Lambda_B) = \frac{8\pi^2}{3|\lambda(\Lambda_B)|} \tag{9}$$

is the action of bounce of size $R = \Lambda_B^{-1}$. Tunneling is dominated by that R for which $S(\Lambda_B)$ is minimum, *i.e.,* when $\lambda(\Lambda_B)$ is minimum, implying $\beta_\lambda(\Lambda_B) = 0$. For a given set of model parameters, in our analysis, Λ_B is determined from the constraining conditions like $\beta_\lambda(\Lambda_B) = 0$, $\lambda(\Lambda_B) = 0$ *etc.* whenever applicable.

The action S receives one-loop correction ΔS, which is rather insignificant [53] when we set the running scale $\mu = 1/R$. The correction due to gravitation $\Delta S_G = 256\pi^3 \Lambda_B^2/45 \left(M_{\rm Pl}\lambda\right)^2$ [54,55] is relevant only when $\Lambda_B \sim M_{\rm Pl}$. In this work, we neglect both of these contributions.

$\mathcal{P}_0 < 1$ corresponds to a vacuum decay lifetime greater than the lifetime of the Universe, $\tau_U \simeq 0.96/H_0 \sim 13.7$ billion years, which in turn implies [53],

$$\lambda(\Lambda_B) > \lambda_{\rm min}(\Lambda_B) = \frac{-0.06488}{1 - 0.00986 \ln\left(v/\Lambda_B\right)} \,. \tag{10}$$

In passing, we note the following:

- If $\lambda(\Lambda_B) > \frac{4\pi}{3}$, $|\kappa| > 8\pi$, $|\lambda_S| > 8\pi$[‡] then the theory is nonperturbative [56–58].
- If $\lambda(\Lambda_B) > 0$, then the vacuum is stable.
- If $0 > \lambda(\Lambda_B) > \lambda_{\rm min}(\Lambda_B)$, then the vacuum is metastable.

[‡]Note that these numbers differ from the ones used in ref. [12].

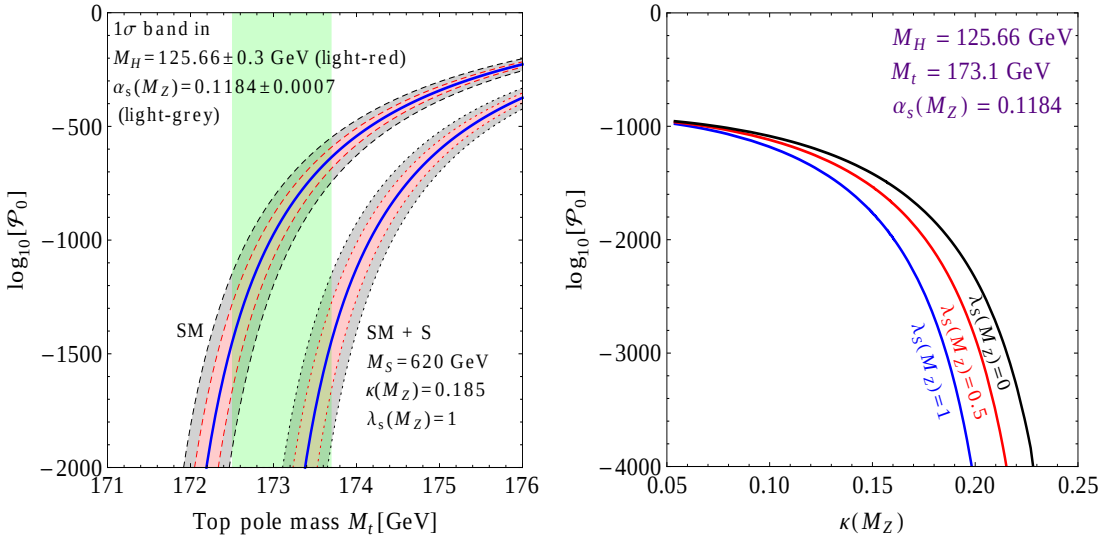

(a) (b)

Figure 4: (**a**) *Tunneling probability* $\mathcal{P}_0$ *as a function of* M_t. *The left band corresponds to* SM *and the right one to* SM+S *for our benchmark point. Light-green band stands for* M_t *at* $\pm 1\sigma$. (**b**) $\mathcal{P}_0$ *as a function of* $\kappa(M_Z)$ *for various* $\lambda_S(M_Z)$.

- If $\lambda(\Lambda_B) < \lambda_{\rm min}(\Lambda_B)$, then the vacuum is unstable.
- If $\lambda_S < 0$, the potential is unbounded from below along the S-direction.
- If $\kappa < 0$, the potential is unbounded from below along a direction in between S and H.

In Fig. 4 we have plotted tunneling probability $\mathcal{P}_0$ as a function of M_t. To calculate $\mathcal{P}_0$, we first find the minimum value of $\lambda_{\rm eff}$ and put the same in eqn. (9) to minimise $S(\Lambda_B)$. The right band corresponds to the tunneling probability for our benchmark point. For comparison, we plot the same for SM as the left band in Fig. 4(a). 1σ error bands in α_S and in M_H are also displayed. The error due to α_S is clearly more significant[§] than that due to M_H. We observe that for a given M_t, these new physics effects lower the tunneling probability. It bolsters our earlier observation that scalar S helps the EW vacuum to come out of metastability. We demonstrate this in Fig. 4(b), where we plot $\mathcal{P}_0$ as a function of $\kappa(M_Z)$ for different choices of $\lambda_S(M_Z)$, assuming central values for M_H, M_t and α_S. We see that for low values of $\kappa(M_Z)$, $\mathcal{P}_0$ tends to coincide with its SM value. For a given $\kappa(M_Z)$, for higher $\lambda_S(M_Z)$, $\mathcal{P}_0$ gets smaller, making the EW vacuum more stable.

[§]There is a typo in Fig. 7 of ref. [9]. The bands due to α_S and M_H have been interchanged.

4 Phase diagrams

The stability of EW vacuum is best displayed with the aid of phase diagrams. We present phase diagrams in different parameter planes for our model.

4.1 $M_H - M_t$ phase diagram

To draw the phase diagram in $M_H - M_t$ plane, we need to identify regions pertaining to EW vacuum stability, metastability and unstable regions. The line separating the stable region from the metastable one is obtained when the two vacua are at the same depth, implying $\lambda(\Lambda_B) = \beta_\lambda(\Lambda_B) = 0$. The unstable region is differentiated from the metastability region by the boundary line where $\beta_\lambda(\Lambda_B) = 0$ along with $\lambda(\Lambda_B) = \lambda_{\rm min}(\Lambda_B)$, defined in eqn. (10).

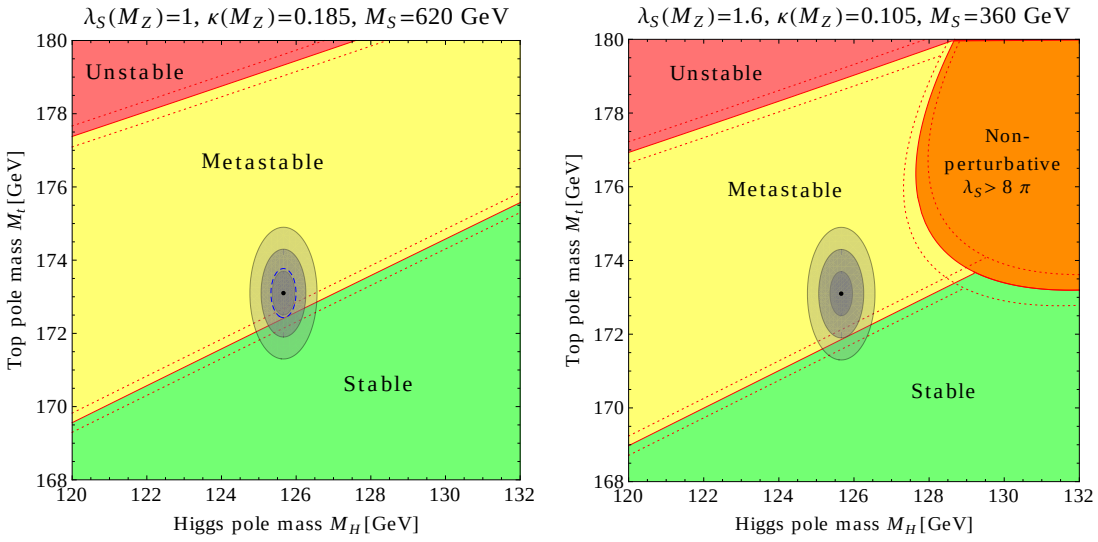

(a) (b)

Figure 5: (**a**) *In* SM+S*, regions of absolute stability (green), metastability (yellow), instability (red) of the EW vacuum in the* $M_H - M_t$ *plane phase diagram is presented for our benchmark point* $M_S = 620$ *GeV,* $\kappa(M_Z) = 0.185$ *and* $\lambda_S(M_Z) = 1$*.* (**b**) *Similar plot for* $M_S = 360$ *GeV,* $\kappa(M_Z) = 0.105$ *and* $\lambda_S(M_Z) = 1.6$*. The orange region corresponds to nonperturbative zone for* λ_S*. The three boundary lines (dotted, solid and dotted red) correspond to* $\alpha_s(M_Z) = 0.1184 \pm 0.0007$*. The grey areas denote the experimentally favoured zones for* M_H *and* M_t *at* 1, 2 *and* 3σ*.*

In the SM, the phase diagram in $M_H - M_t$ plane is given in refs. [9, 29]. Our results agree with them. Given the measured errors on $M_t = 173.1 \pm 0.6$ GeV and M_H, the SM phase diagram indicates that the stability of EW vacuum is excluded

at $\sim 3\sigma$[¶]. However, the extra scalar in our model modifies these findings.

We present the phase diagram in the $M_H - M_t$ plane for SM+S in Fig. 5. For our benchmark point, we see that the boundaries shift towards higher values of M_t, so that the EW vacuum stability is excluded only at 1.1σ, indicated by the blue-dashed ellipse. For $M_S = 360$ GeV, $\kappa(M_Z) = 0.105$ and $\lambda_S(M_Z) = 1.6$, the plot is redrawn to highlight the fact that λ_S might turn out to be too large, so that the theory becomes nonperturbative (marked as the orange region in Fig. 5(b)). Here EW vacuum stability is excluded at 2σ. All these boundaries separating various stability regions in the phase diagram depend on α_S. 1σ bands for the same is also displayed in these figures.

4.2 Confidence level of vacuum stability

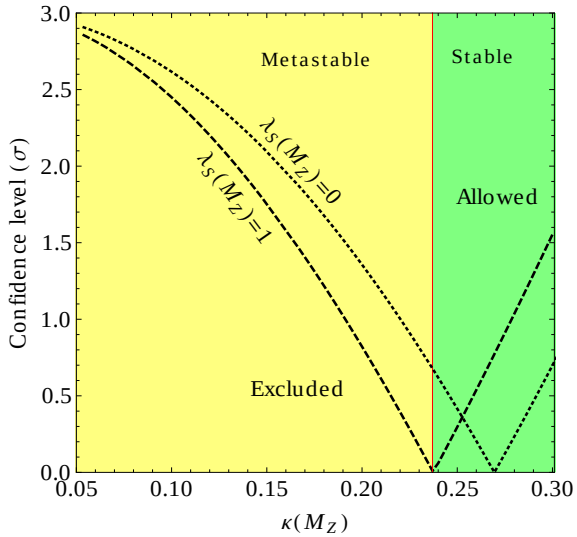

Figure 6: *Dependence of confidence level (one-sided) at which EW vacuum stability is excluded/allowed on $\kappa(M_Z)$. Regions of absolute stability (green) and metastability (yellow) of EW vacuum are shown.*

As new physics effects do change the stability of EW vacuum, it is important to show the change in the confidence level at which stability is excluded or allowed. In Fig. 6, we plot confidence level against $\kappa(M_Z)$ for $M_t = 173.1$ GeV, $M_H = 125.66$ GeV and $\alpha_S(M_Z) = 0.1184$. M_S is dictated by $\kappa(M_Z)$ to satisfy $\Omega_{\rm DM}h^2 \approx 0.1198$. For $\lambda_S(M_Z) = 1$, we see that the EW vacuum becomes stable for $\kappa(M_Z) = 0.24$ onward. For a lower $\lambda_S(M_Z)$, this point shifts to a higher value. If $\lambda_S(M_Z) = 0$, stability is assured for $\kappa(M_Z) \geq 0.27$. Note that as κ dependence in RGE running of λ creeps in through the term $\kappa^2/2$ in β_λ, the stability strongly depends on $\kappa(M_Z)$. However, as

[¶]In a mass dependent renormalisation scheme, such exclusion happens at 3.5σ [59].

β_λ depends on λ_S only *via* κ running, although λ_S running is relatively strong, the stability of EW vacuum does not change appreciably when $\lambda_S(M_Z)$ is varied from 0 to 1.

4.3 $M_t - \alpha_S(M_Z)$ phase diagram

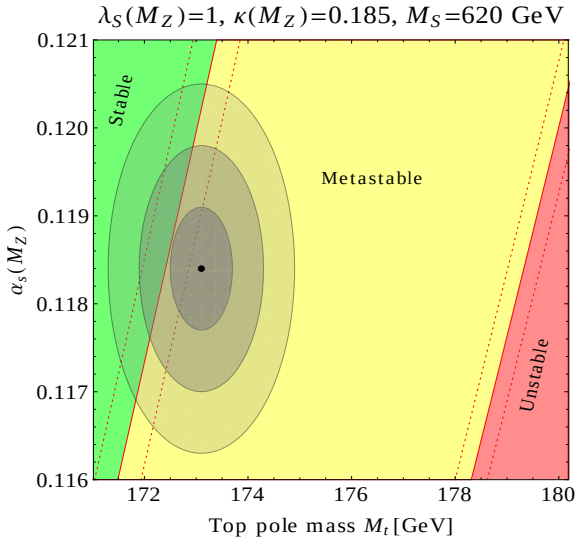

Figure 7: *Phase diagram in $M_t - \alpha_S(M_Z)$ plane in* SM+S *model for our benchmark point. Regions of absolute stability (green), metastability (yellow), instability (red) of the EW vacuum are marked. The dotted lines correspond to $\pm 3\sigma$ variation in M_H and the grey areas denote the experimental allowed region for M_t and $\alpha_S(M_Z)$ at 1, 2 and 3σ.*

Given the sizable error on $\alpha_S(M_Z)$, it is instructive to draw the phase diagram in the $M_t - \alpha_S(M_Z)$ plane as well. This diagram for SM is available in refs. [10,60]. We present the same in Fig. 7 for our model using our benchmark point. With increase of $\kappa(M_Z)$ and/or $\lambda_S(M_Z)$, the boundaries between different stability regions shift towards right, allowing the EW vacuum to be more stable.

4.4 Asymptotic safety

Shaposhnikov and Wetterich predicted [61] mass of the Higgs boson of 126 GeV imposing the constraint $\lambda(M_{\rm Pl}) = \beta_\lambda(M_{\rm Pl}) = 0$, in a scenario known as asymptotic safety of gravity. As mentioned before, this corresponds to two degenerate vacua. In ref. [29], it was clearly shown that the present error in M_t and M_H does not allow this condition to be realised in SM. In SM+S model, the situation worsens [12] and we demonstrate this in Fig. 8(a) for our benchmark point. In presence of the scalar,

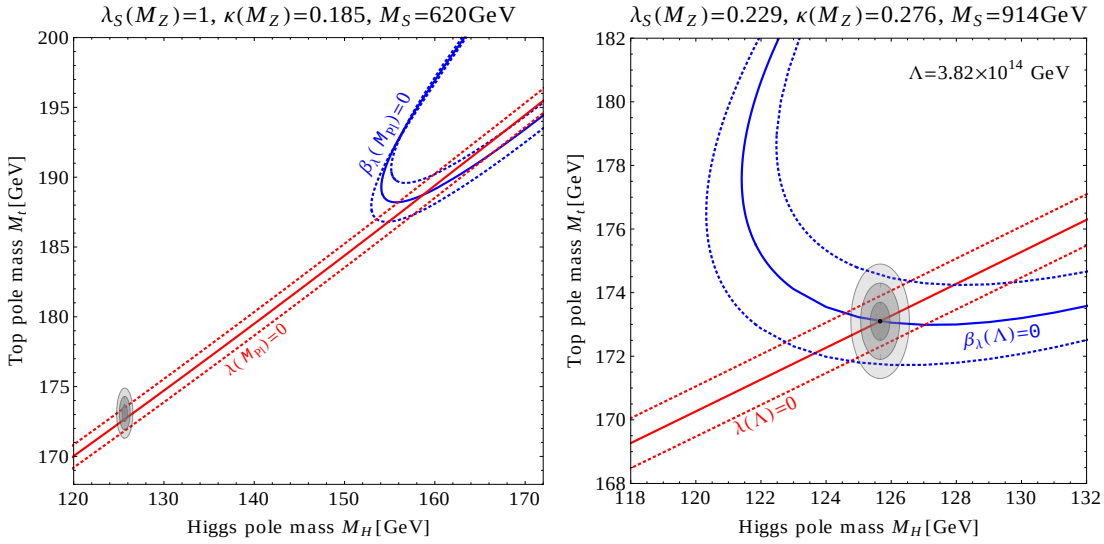

(a) (b)

Figure 8: (**a**) *Contour plot for* $\lambda(M_{\rm Pl}) = 0$ *(red line) and* $\beta_\lambda(M_{\rm Pl}) = 0$ *(blue line) for our benchmark point.* (**b**) *Similar plot for* $\lambda(\Lambda) = 0$ *and* $\beta_\lambda(\Lambda) = 0$*, where* $\Lambda = 3.8 \times 10^{14}$ *GeV. Dotted lines correspond to* $\pm 3\sigma$ *variation in* $\alpha_s(M_Z)$*. The grey areas denote the experimental allowed region for* M_H *and* M_t *at* 1, 2 *and* 3σ*.*

the values of M_t and M_H, required to satisfy this condition, are pushed far away from the experimentally favoured numbers: For our benchmark point this condition is satisfied at $M_H = 140.8$ GeV and $M_t = 179.5$ GeV.

However, it is possible to meet this condition at a lower energy than at $M_{\rm Pl}$. In Fig. 8(b), it is demonstrated that at a different point in the parameter space: $M_S = 914$ GeV, $\kappa(M_Z) = 0.276$ and $\lambda_S(M_Z) = 0.229$, the condition $\lambda(\Lambda) = \beta_\lambda(\Lambda) = 0$ is indeed satisfied at $\Lambda = 3.8 \times 10^{14}$ GeV and is also consistent with experimentally allowed range for M_t and M_H. The value of Λ decreases with $\lambda_S(M_Z)$ and $\kappa(M_Z)$. The corresponding value of M_S is chosen to satisfy relic density of DM constraints. Also, it is difficult to simultaneously satisfy Veltman condition at $M_{\rm Pl}$ [12]. All these observations indicate that some new physics could be operational at very high energies to take care of such issues.

4.5 $\kappa(M_Z) - M_S$ phase diagram

The phase diagram for $\kappa(M_Z) - M_S$ plane is displayed in Fig. 9. As addition of the scalar does not drive the EW vacuum towards instability, there is no unstable region marked on the plot. Between the dashed lines, we mark the allowed region ensuing from relic density constraints. For $M_S > 100$ GeV, $SS \to W^+W^-$ [62] dominates over other DM annihilation channels. Under the approximation $M_S \gg M_W, M_H$, in

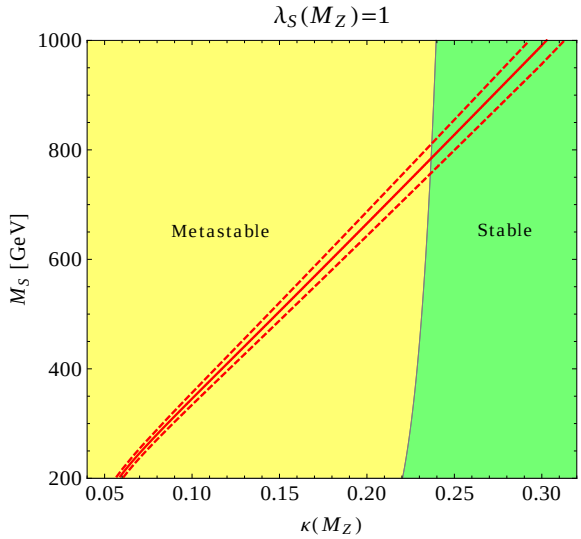

Figure 9: *Phase diagram in $\kappa(M_Z) - M_S$ plane. Regions of absolute stability (green), metastability (yellow) of the EW vacuum for $\lambda_S(M_Z) = 1$ are shown. The red solid line corresponds to $\Omega_{\rm DM}h^2 \approx 0.1198$. The red dashed lines correspond to 3σ error on $\Omega_{\rm DM}h^2$.*

the non-relativistic limit,

$$\sigma(SS \to W^+W^-) \propto \frac{\kappa^2}{M_S^2}\,. \tag{11}$$

Hence, to satisfy relic density constraints, $\kappa(M_Z)$ depends linearly on M_S as shown in Fig. 9.

4.6 $\kappa(M_Z) - M_H$ phase diagram

In SM, the vacuum stability bound

$$M_H\ [\text{GeV}] > 129.46 + 1.12\left(\frac{M_t\ [\text{GeV}] - 173.1}{0.6}\right) - 0.56\left(\frac{\alpha_S(M_Z) - 0.1184}{0.0007}\right) \tag{12}$$

is obtained from the requirement $\lambda = \beta_\lambda = 0$. The metastability bound

$$M_H\ [\text{GeV}] > 109.73 + 1.84\left(\frac{M_t\ [\text{GeV}] - 173.1}{0.6}\right) - 0.88\left(\frac{\alpha_S(M_Z) - 0.1184}{0.0007}\right) \tag{13}$$

comes from the requirement $\beta_\lambda = 0$ and $\lambda = \lambda_{\rm min}$. To ensure perturbativity, we demand $\lambda(M_{\rm Pl}) < \frac{4\pi}{3}$, which leads to

$$M_H\ [\text{GeV}] < 172.23 + 0.36\left(\frac{M_t\ [\text{GeV}] - 173.1}{0.6}\right) - 0.12\left(\frac{\alpha_S(M_Z) - 0.1184}{0.0007}\right)\,. \tag{14}$$

Now, let us see what happens in SM+S model. In this context, change in M_H bounds with respect to $\kappa(M_Z)$ was considered in refs. [16, 28] for different cut-off

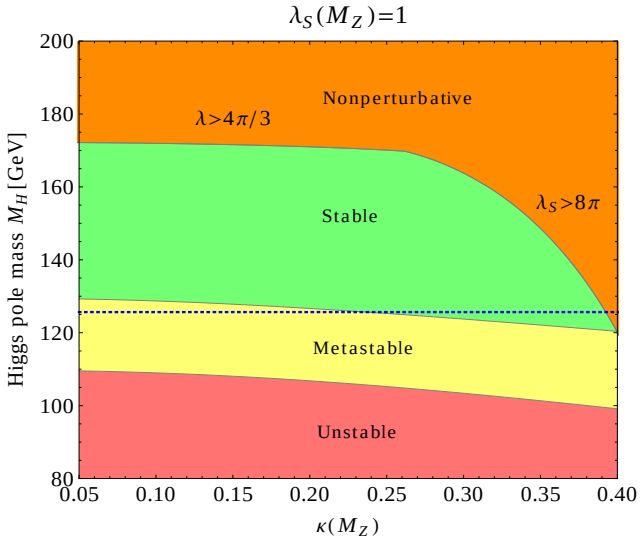

Figure 10: *Phase diagram in $\kappa(M_Z) - M_H$ plane. Regions of absolute stability (green), metastability (yellow) and instability (red) of the EW vacuum for $\lambda_S(M_Z) = 1$ are displayed. λ and/or λ_S are/is nonperturbative in the orange region. The blue dashed line corresponds to $M_H = 125.66$ GeV.*

scales, considering stability aspects only. As shown in Fig. 10, in presence of the scalar S, these bounds shift to lower values for larger $\kappa(M_Z)$. For large values of $\kappa(M_Z)$, depending on our choice of λ_S at M_Z, $\lambda_S(M_{\rm Pl})$ may become so large that the theory becomes nonperturbative. This imposes further constraints on the parameter space, shown as the curved line representing $\lambda_S(M_{\rm Pl}) = 8\pi$. As before, for a given $\kappa(M_Z)$, M_S is chosen in such a way that $\Omega_{\rm DM}h^2 \approx 0.1198$ for $M_H = 125.66$ GeV. However, in the plot, as M_H changes, $\Omega_{\rm DM}h^2$ also changes. But this variation is contained within 3σ.

5 Discussion and conclusion

According to the standard model of particle physics, the electroweak vacuum is lying right in between stability and instability, as if, it is ready to tunnel into a regime of absolute instability. Nevertheless, the transition time required for this is safely beyond the present lifetime of the Universe. Still, the question is, what prompts such a near-criticality? In this paper, we did not try to find an answer to this question. But we explored the validity of this question in the context of an extended model containing a singlet scalar dark matter.

Near-criticality is best explained with the help of phase diagrams. Refs. [9, 10, 29] demonstrated quite a few of them to explain metastability in SM. We made a similar endeavour in the SM+S model. We included NNLO corrections in our SM

calculations, but the effects due to the scalar S were incorporated at the level of one-loop only.

We chose a dark matter model to illustrate changes in EW vacuum stability as apart from neutrino masses, the presence of dark matter in the Universe is the most striking signature of new physics beyond the standard model of particle physics. SM+S is the simplest dark matter model one can work with. The present work deals with DM mass of 200 GeV or more. The work can be extended to lower DM masses as well. However, in this case, to satisfy DM relic density constraints, $\kappa(M_Z)$ will also be small, leading to little deviation in the EW vacuum metastability from the SM case.

Non-observation of any signature pertaining to supersymmetry or extra dimensions or any other TeV scale physics at LHC has led us to cast doubt on our take on the naturalness issues associated with the Higgs sector. It has led to a possibility that SM is not an effective field theory, but a fundamental theory of Nature, valid up to the Planck scale. To explain dark matter, here we assumed the singlet scalar extended SM reigns up to $M_{\rm Pl}$ as well. One need not be concerned about the hierarchy problem as we assume that Planck scale physics somehow takes care of that. In any case, as new scalars are of mass within a TeV, we are not introducing any new hierarchy problem in traditional sense. As the Higgs potential seems to vanish around $M_{\rm Pl}$, it has led to speculations [5, 61, 63–68] regarding the underlying dynamics operational at very high energies.

In SM+S, for some specific choice of parameter space, the scalar S can rescue the EW vacuum from metastability, making it absolutely stable, so that λ never turns negative. But as the DM direct detection experiments or collider searches are yet to confirm the exact nature of DM candidate, we consider the parameter space allowed by DM relic density constraints, dictated by the CMBR experiments such as Planck or WMAP. We have checked that in all our considerations, the DM $-$ nucleon cross-sections are beyond the present sensitivity of direct detection experiments such as XENON100 and LUX.

In SM at $\Lambda_I \sim 10^{10}$ GeV, λ vanish and becomes negative at higher energies. As β_λ also becomes very small at high energies, it forbids λ to attain a large negative value and thus protects the EW vacuum to go through a quick transition towards instability. As $\lambda \to 0$ does not add to any known symmetry, we are not sure of the exact nature of new dynamics it is pointing to, or it could just be a fortuitous numerical coincidence. We observed that for our benchmark point, Λ_I shifts by around an order of magnitude. So, the energy at which this unknown dynamics starts its action gets deferred in presence of the scalar S. Addition of S does not help in realising the asymptotic safety scenario of gravity. But it is possible to have two degenerate vacua at somewhat lower energy, which depends on the parameter

space under consideration.

In short, near-criticality of EW vacuum indicates presence of new dynamics other than the SM at a very high energy. In this work, we do not speculate about the nature such new physics, but introduce scalars at lower energies to demonstrate the influence of such scalars in shaping the minimum (if any) of the potential lying close to $M_{\rm Pl}$. In particular, we had shown that the onset scale of such high-energy dynamics may differ and the bounds on M_H from stability considerations do change, in presence of these new scalars.

Acknowledgments

The work of NK is supported by a fellowship from UGC. SR acknowledges support of seed grant from IIT Indore. NK also acknowledges private communications with G. Isidori, A. Strumia and M.F. Zoller. SR is grateful to S. Raychaudhuri for discussions.

References

[1] G. Aad *et al.* [ATLAS Collaboration], Phys. Lett. B **716**, (2012) 1 [arXiv:1207.7214 [hep-ex]].

[2] S. Chatrchyan *et al.* [CMS Collaboration], Phys. Lett. B **716**, (2012) 30 [arXiv:1207.7235 [hep-ex]].

[3] P. P. Giardino, K. Kannike, I. Masina, M. Raidal and A. Strumia, JHEP **1405**, (2014) 046 [arXiv:1303.3570 [hep-ph]].

[4] G. F. Giudice, PoS EPS-HEP2013, (2013) 163 [arXiv:1307.7879 [hep-ph]].

[5] M. Holthausen, J. Kubo, K. S. Lim and M. Lindner, JHEP **1312**, (2013) 076 [arXiv:1310.4423 [hep-ph]].

[6] W. A. Bardeen, FERMILAB-CONF-95-391-T.

[7] S. R. Coleman and E. J. Weinberg, Phys. Rev. D **7**, (1973) 1888.

[8] M. Sher, Phys. Rept. **179**, (1989) 273.

[9] D. Buttazzo, G. Degrassi, P. P. Giardino, G. F. Giudice, F. Sala, A. Salvio and A. Strumia, JHEP **1312**, (2013) 089 [arXiv:1307.3536 [hep-ph]].

[10] F. Bezrukov, M. Y. Kalmykov, B. A. Kniehl and M. Shaposhnikov, JHEP **1210**, (2012) 140 [arXiv:1205.2893 [hep-ph]].

[11] C. P. Burgess, M. Pospelov and T. ter Veldhuis, Nucl. Phys. B **619**, (2001) 709 [hep-ph/0011335].

[12] N. Haba, K. Kaneta and R. Takahashi, JHEP **1404**, (2014) 029 [arXiv:1312.2089 [hep-ph]].

[13] M. Kadastik, K. Kannike, A. Racioppi and M. Raidal, JHEP **1205**, (2012) 061 [arXiv:1112.3647 [hep-ph]].

[14] C. -S. Chen and Y. Tang, JHEP **1204**, (2012) 019 [arXiv:1202.5717 [hep-ph]].

[15] E. Gabrielli, M. Heikinheimo, K. Kannike, A. Racioppi, M. Raidal and C. Spethmann, Phys. Rev. D **89**, (2014) 015017 [arXiv:1309.6632 [hep-ph]].

[16] M. Gonderinger, Y. Li, H. Patel and M. J. Ramsey-Musolf, JHEP **1001**, (2010) 053 [arXiv:0910.3167 [hep-ph]].

[17] T. E. Clark, B. Liu, S. T. Love and T. ter Veldhuis, Phys. Rev. D **80**, (2009) 075019 [arXiv:0906.5595 [hep-ph]].

[18] R. N. Lerner and J. McDonald, Phys. Rev. D **80**, (2009) 123507 [arXiv:0909.0520 [hep-ph]].

[19] C. Cheung, M. Papucci and K. M. Zurek, JHEP **1207**, (2012) 105 [arXiv:1203.5106 [hep-ph]].

[20] O. Lebedev, Eur. Phys. J. C **72**, (2012) 2058 [arXiv:1203.0156 [hep-ph]].

[21] J. Elias-Miro, J. R. Espinosa, G. F. Giudice, H. M. Lee and A. Strumia, JHEP **1206**, (2012) 031 [arXiv:1203.0237 [hep-ph]].

[22] O. Antipin, J. Krog, M. Mojaza and F. Sannino, Nucl. Phys. B **886**, 125 (2014) [arXiv:1311.1092 [hep-ph]].

[23] S. Khan, S. Goswami and S. Roy, Phys. Rev. D **89**, (2014) 073021 [arXiv:1212.3694 [hep-ph]].

[24] B. Grzadkowski and J. Wudka, Phys. Rev. Lett. **88**, (2002) 041802 [hep-ph/0106233].

[25] V. Branchina and E. Messina, Phys. Rev. Lett. **111**, (2013) 241801 [arXiv:1307.5193 [hep-ph]].

[26] Z. Lalak, M. Lewicki and P. Olszewski, JHEP **1405**, (2014) 119 [arXiv:1402.3826 [hep-ph]].

[27] V. Branchina, E. Messina and A. Platania, arXiv:1407.4112 [hep-ph].

[28] A. Eichhorn and M. M. Scherer, Phys. Rev. D **90**, 025023 (2014) [arXiv:1404.5962 [hep-ph]].

[29] G. Degrassi, S. Di Vita, J. Elias-Miro, J. R. Espinosa, G. F. Giudice, G. Isidori and A. Strumia, JHEP **1208**, (2012) 098 [arXiv:1205.6497 [hep-ph]].

[30] I. Masina, Phys. Rev. D **87**, (2013) 053001 [arXiv:1209.0393 [hep-ph]].

[31] M. Gonderinger, H. Lim and M. J. Ramsey-Musolf, Phys. Rev. D **86**, (2012) 043511 [arXiv:1202.1316 [hep-ph]].

[32] J. A. Casas, J. R. Espinosa and M. Quiros, Phys. Lett. B **342**, (1995) 171 [hep-ph/9409458].

[33] G. Altarelli and G. Isidori, Phys. Lett. B **337**, (1994) 141.

[34] J. A. Casas, J. R. Espinosa, M. Quiros and A. Riotto, Nucl. Phys. B **436**, (1995) 3 [Erratum-ibid. B **439**, (1995) 466] [hep-ph/9407389].

[35] J. A. Casas, J. R. Espinosa and M. Quiros, Phys. Lett. B **382**, (1996) 374 [hep-ph/9603227].

[36] M. Quiros, hep-ph/9703412.

[37] C. Ford, I. Jack and D. R. T. Jones, Nucl. Phys. B **387**, (1992) 373 [Erratum-ibid. B **504**, (1997) 551] [hep-ph/0111190].

[38] S. P. Martin, Phys. Rev. D **65**, (2002) 116003 [hep-ph/0111209].

[39] L. N. Mihaila, J. Salomon and M. Steinhauser, Phys. Rev. Lett. **108**, (2012) 151602 [arXiv:1201.5868 [hep-ph]].

[40] K. G. Chetyrkin and M. F. Zoller, JHEP **1206**, (2012) 033 [arXiv:1205.2892 [hep-ph]].

[41] M. F. Zoller, arXiv:1209.5609 [hep-ph].

[42] K. G. Chetyrkin and M. F. Zoller, JHEP **1304**, (2013) 091 [Erratum-ibid. **1309**, (2013) 155] [arXiv:1303.2890 [hep-ph]].

[43] M. Zoller, PoS EPS-HEP2013, (2014) 322 [arXiv:1311.5085 [hep-ph]].

[44] H. Davoudiasl, R. Kitano, T. Li and H. Murayama, Phys. Lett. B **609**, (2005) 117 [hep-ph/0405097].

[45] A. Sirlin and R. Zucchini, Nucl. Phys. B **266**, (1986) 389.

[46] K. Melnikov and T. v. Ritbergen, Phys. Lett. B **482**, (2000) 99 [hep-ph/9912391].

[47] M. Holthausen, K. S. Lim and M. Lindner, JHEP **1202**, (2012) 037 [arXiv:1112.2415 [hep-ph]].

[48] P. A. R. Ade *et al.* [Planck Collaboration], Astron. Astrophys. (2014) [arXiv:1303.5076 [astro-ph.CO]].

[49] A. Alloul, N. D. Christensen, C. Degrande, C. Duhr and B. Fuks, Comput. Phys. Commun. **185**, (2014) 2250 [arXiv:1310.1921 [hep-ph]].

[50] G. Belanger, F. Boudjema, P. Brun, A. Pukhov, S. Rosier-Lees, P. Salati and A. Semenov, Comput. Phys. Commun. **182**, (2011) 842 [arXiv:1004.1092 [hep-ph]].

[51] G. Belanger, F. Boudjema, A. Pukhov and A. Semenov, Comput. Phys. Commun. **185**, (2014) 960 [arXiv:1305.0237 [hep-ph]].

[52] S. R. Coleman, Phys. Rev. D **15**, (1977) 2929 [Erratum-ibid. D **16**, (1977) 1248].

[53] G. Isidori, G. Ridolfi and A. Strumia, Nucl. Phys. B **609**, (2001) 387 [hep-ph/0104016].

[54] S. R. Coleman and F. De Luccia, Phys. Rev. D **21**, (1980) 3305.

[55] G. Isidori, V. S. Rychkov, A. Strumia and N. Tetradis, Phys. Rev. D **77**, (2008) 025034 [arXiv:0712.0242 [hep-ph]].

[56] B. W. Lee, C. Quigg and H. B. Thacker, Phys. Rev. D **16**, (1977) 1519.

[57] G. Cynolter, E. Lendvai and G. Pocsik, Acta Phys. Polon. B **36**, (2005) 827 [hep-ph/0410102].

[58] K. P. Modak, D. Majumdar and S. Rakshit, arXiv:1312.7488 [hep-ph].

[59] A. Spencer-Smith, arXiv:1405.1975 [hep-ph].

[60] J. Elias-Miro, J. R. Espinosa, G. F. Giudice, G. Isidori, A. Riotto and A. Strumia, Phys. Lett. B **709**, (2012) 222 [arXiv:1112.3022 [hep-ph]].

[61] M. Shaposhnikov and C. Wetterich, Phys. Lett. B **683**, (2010) 196 [arXiv:0912.0208 [hep-th]].

[62] J. McDonald, Phys. Rev. D **50**, (1994) 3637 [hep-ph/0702143].

[63] C. D. Froggatt and H. B. Nielsen, Phys. Lett. B **368**, (1996) 96 [hep-ph/9511371].

[64] M. Hashimoto, S. Iso and Y. Orikasa, Phys. Rev. D **89**, (2014) 016019 [arXiv:1310.4304 [hep-ph]].

[65] R. Foot, A. Kobakhidze, K. L. McDonald and R. R. Volkas, Phys. Rev. D **89**, (2014) 115018 [arXiv:1310.0223 [hep-ph]].

[66] M. Ibe, S. Matsumoto and T. T. Yanagida, Phys. Lett. B **732**, (2014) 214 [arXiv:1312.7108 [hep-ph]].

[67] A. Kobakhidze and K. L. McDonald, JHEP **1407**, 155 (2014) [arXiv:1404.5823 [hep-ph]].

[68] N. Haba, H. Ishida, K. Kaneta and R. Takahashi, Phys. Rev. D **90**, 036006 (2014) [arXiv:1406.0158 [hep-ph]].